

Enhancing Organolead Halide Perovskite Solar Cells Performance Through Interfacial Engineering Using Ag-doped TiO₂ Hole Blocking Layer

Ming-Chung Wu,* Ying-Han Liao, Shun-Hsiang Chan, Chun-Fu Lu, and Wei-Fang Su

Various silver-doped titanium dioxide (Ag-TiO₂) hole blocking layers are used to improve the organolead halide perovskite-structured solar cells (PSCs) performances. In this work, a series of Ag-TiO₂ compact layers with various dopant levels are successfully synthesized, and they are used to fabricate PSCs. The silver doping effects on the morphology and physical properties of Ag-TiO₂ compact layers are studied using X-ray diffractometer, UV-visible spectroscopy, contact angle meter, scanning electron microscope, atomic force microscope, and time-resolved photoluminescence spectroscopy. Furthermore, the photo-assisted Kelvin probe force microscopy is used to monitor the surface potentials. With 1.0 mol% Ag-TiO₂ PSCs, the short-circuit current density increases notably because of the lower electron–hole recombination, which increases the electron injection. After optimizing the synthesis conditions, the champion device based on 1.0 mol% Ag-TiO₂ exhibits a power conversion efficiency of 14.1% under AM 1.5 G irradiation (100 mW · cm⁻²).

characteristics, including high power conversion efficiency (PCE), easy fabrication, and low-cost. Miyasaka group reported the first PSCs with a PCE of ≈3.8%.^[1] After that, the PCE of PSCs has rapidly increased to 22.7% in the last decade.^[2,3] The n-i-p structure is commonly used to fabricate the planar methylammonium lead halide perovskite-structured photovoltaic device with an architecture of glass/F:SnO₂ (FTO)/TiO₂/CH₃NH₃PbX₃/spiro-OMeTAD/metal electrode.^[4–5] The organolead halide perovskite-structured material usually acts as the light-harvesting material^[3,6–9] and exhibits the high carrier mobility. In addition, TiO₂ is applied as the planar hole blocking layer due to its cost-effectiveness, chemical inertness, optical stability, non-toxicity, and high carrier mobility.^[10–15] The photoexcited electrons tend to transfer from perovskite-structured active layer to TiO₂ hole blocking layer.^[16] Hence, a further dop-

1. Introduction

Organolead halide perovskite-structured solar cells (PSCs) have been developed and frequently optimized on account of their

ing of metal ions into TiO₂ can tune the optical characteristics, and also improve the separation of electron–hole pairs.^[17–19]

Y. Shi et al. compared the photovoltaic characteristics of the PSCs constructed by CH₃NH₃PbI_{3-x}Cl_x as the perovskite-structured active layer and accompanied with a planar TiO₂ or mesoporous TiO₂ as the hole blocking layer. The CH₃NH₃PbI_{3-x}Cl_x PSCs exhibited a PCE of 12.67 and 7.87%, with the planar TiO₂ and the mesoporous TiO₂ as hole blocking layer, respectively.^[20] The CH₃NH₃PbI_{3-x}Cl_x PSCs exhibit a longer electron diffusion length and could form a highly crystalline perovskite-structured active layer.^[21–22] Therefore, we chose the CH₃NH₃PbI_{3-x}Cl_x as the perovskite-structured active layer accompanied with planar TiO₂ to obtain an extraordinary photovoltaic performance in this study.


For the hole blocking layer of PSCs, doping TiO₂ with non-metal (e.g., N and F)^[23–24] or metal (e.g., Cs, Sn, Cd, Au, W, Nb, and Zn)^[25–31] can significantly extend the optical absorption toward visible light band and enhance the carrier mobility. With the suitable dopant, it could tune the TiO₂ bandgap and accelerate the separation of photo-induced electrons and holes. For the non-metal doped TiO₂ hole blocking layer, N-doped TiO₂ nanorods exhibits the enhanced absorption behavior compared with pristine TiO₂, by decreasing the band gap from 3.03 to 2.74 eV. Also, the small

Prof. M.-C. Wu, Y.-H. Liao, S.-H. Chan
Department of Chemical and Materials Engineering
Chang Gung University
Taoyuan 33302, Taiwan
E-mail: mingchungwu@mail.cgu.edu.tw

Prof. M.-C. Wu
Centre for Reliability Science and Technologies
Chang Gung University
Taoyuan 33302, Taiwan

Prof. M.-C. Wu
Division of Neonatology, Department of Pediatrics
Chang Gung Memorial Hospital, Linkuo
Taoyuan 33305, Taiwan

C.-F. Lu, Prof. W.-F. Su
Department of Materials Science and Engineering
National Taiwan University
Taipei 10617, Taiwan

 The ORCID identification number(s) for the author(s) of this article can be found under <https://doi.org/10.1002/solr.201800072>.

DOI: 10.1002/solr.201800072

band gap can result in the offset of the conduction band and can enhance the PCE.^[24] F-doped TiO₂ can enhance the photovoltaic characteristic of PSCs due to the enlarge of electrical conductivity and photoluminescence behavior.^[23] Doping metal ion into TiO₂ hole blocking layer is a conventional method to enhance the photovoltaic characteristic. Based on the study of interfacial engineering, using Cs-doped TiO₂ as a hole blocking layer for planar PSCs could achieve the PCE of ≈5.26% due to the decreased interfacial resistance with an increased conduction band maximum.^[27] The PSC with Sn-doped TiO₂ nanorods shows the high light-capture ability and the high carrier mobility, and its PCE of ≈6.3% is almost 67% higher than that of pristine TiO₂ nanorod of 3.78% under the same condition.^[25] Cd-doped TiO₂ nanorod arrays are also adopted to enhance the open circuit voltage, and their PCE can achieve 8.3%, which is almost 30% higher than that of the pristine TiO₂.^[27] Au-doped TiO₂ PSC shows the conduction band approaching the perovskite-structured active layer that results in the high charge separation, and its PCE is ≈8.8%.^[28] The W-doped TiO₂ based PSC shows the enlarged energy gap, good electron collection capability, and a high PCE of ≈10.6%.^[29] Through the transient photocurrent decay and impedance studies, the Nb-doped TiO₂ based PSC exhibits a higher PCE of 13.4% than pristine TiO₂ based PSC of 12.2% due to the fast electron transport and preserved electron lifetime.^[31] The Zn-doped TiO₂ based PSC demonstrates its high electrical conductivity and charge separation efficiency, and it shows a high PCE of ≈14.0%.^[26]

The synthesis of Ag-doped TiO₂ has been widely studied in recent decades, and it presents the high-performance optoelectronic characteristics.^[32–36] However, Ag-doped TiO₂ has rarely been used as the planar hole blocking layer of organolead halide PSCs. In this study, we prepare a series of Ag-doped TiO₂ (Ag-TiO₂) hole blocking layers through the sol-gel synthesis. The various Ag-TiO₂ hole blocking layers are further used to fabricate n-i-p structure PSCs. Here, we systematically study the film morphology, optical properties, electrical conductivity, charge carrier dynamics, and photovoltaic characteristic. The PSCs with Ag-TiO₂ hole blocking layer show the enhanced photovoltaic performance and PCE.

2. Results and Discussion

The XRD patterns of various Ag-TiO₂ layers are shown in **Figure 1a**. For pristine TiO₂ layer, all peaks exhibit the body-centered tetragonal structure of anatase TiO₂ [COD ID: 720675]. The full width at half maximum (FWHM) of anatase TiO₂ (101) plane increases with increasing Ag doping level, because the ionic radius of Ag⁺ is larger than Ti⁴⁺ as shown in **Figure 1b**. For the various Ag-TiO₂ with different dopant levels, the primary crystal structure is anatase TiO₂ which indicates that the silver dopant will not change the crystal structure of anatase TiO₂. The comparison of XRD patterns for Ag-TiO₂ with high dopant levels are shown in **Figure S1**, Supporting Information. The diffraction peak of Ag (111) overlaps with anatase TiO₂ (004). When Ag doping level is higher than 3.0 mol%, Ag (200) and Ag (220) diffraction peaks can be observed in the XRD patterns. Hence, the high Ag doping level could cause the decay of PCE due to the existence of impurity in TiO₂ lattice. In addition, the crystallite size for (101) plane of anatase phase TiO₂ is calculated by Debye-Scherrer equation. The crystallite size of the various Ag-TiO₂ layers decreases as the dopant level increases as shown in **Figure 1b** and **Figure 1c**.^[32] Debye-Scherrer equation is shown as below:

$$D = \frac{K\lambda}{\beta \cos \theta} \quad (1)$$

where: D is the calculated mean size of crystalline domains, K is the shape factor (≈ 0.9), λ is the X-ray wavelength ($\approx 1.54 \text{ \AA}$), β and θ are FWHM (in radians) and Bragg angle (in degrees), respectively.

The absorption spectra of Ag-TiO₂ layers show considerable red-shift as shown in **Figure 2a** and **b**. The bandgap decreases from 3.76 to 3.72 eV as Ag doping level increases from 0.0 to 3.0 mol%. The decreased bandgap is due to the importing of new band, in the TiO₂ bandgap, which is form by the existence of Ag ion. The result could also reduce the energy for producing electron-hole pairs. The site of the conduction band could be decreased due to the Ag ion that doped into TiO₂ layer. The change of conduction band position edge could inject the electron efficiently from the active layer to hole blocking layer.^[37]

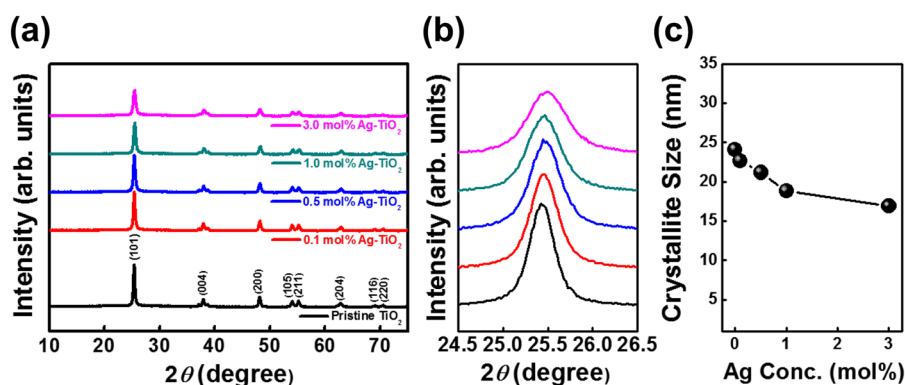


Figure 1. a) XRD patterns, b) the magnified patterns at 2θ ranged from 24.5 to 26.5 degree, and c) the calculated mean size for (101) plane of Ag-TiO₂ layers with various Ag doping levels.

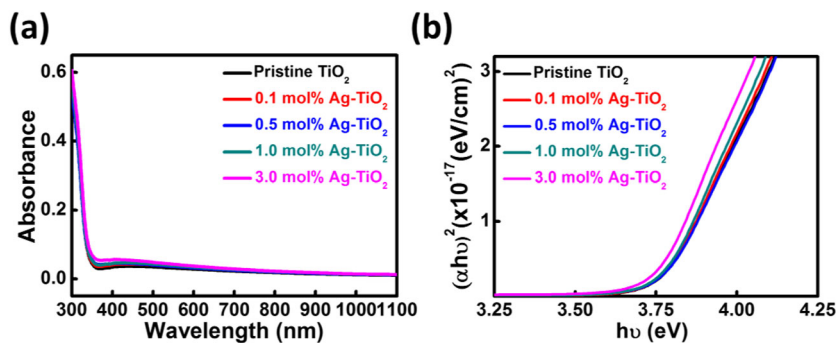


Figure 2. a) UV-visible absorption spectra and b) Tauc plot of pristine TiO₂ and various Ag-TiO₂ layers.

The interface between the active layer and hole blocking layer plays an essential role in the electron transport behavior. Scanning electron microscope (SEM) and atomic force microscope (AFM) were used to observe the topography of TiO₂-based layers with various Ag doping levels, and their images are shown in Figure S2, Supporting Information. As Ag doping level increases from 0.0 to 3.0 mol%, the SEM images show no noteworthy change. **Figure 3a** shows the root mean square (RMS) roughness analysis of Ag-TiO₂ layer. While the Ag doping levels increases from 0.0 to 3.0 mol%, RMS roughness of these layers is similar. Hence, doping Ag into the TiO₂ layer does not increase the roughness when dopant level is lower than 3.0 mol%. However, the contact angles formed by sessile liquid drops on the surface of the various Ag-TiO₂ layer are different as shown in **Figure 3b**. The 1.0 mol% Ag-TiO₂ layer shows the small contact angle which corresponds to high wettability. The organolead halide perovskite precursor used in this study is dissolved in DMF, a hydrophilic aprotic solvent. Therefore, the perovskite-structured active layer could be more uniform by coating the perovskite precursor solution on the high wettable TiO₂ surface. The surface morphologies of perovskite-structured active layer coated on the various Ag-TiO₂ layer are observed by SEM as shown in Figure S3. The perovskite-structured active layer coated on 1.0 mol% Ag-TiO₂ layer shows smooth surface morphology due to the high wettability of 1.0 mol% Ag-TiO₂ layer.

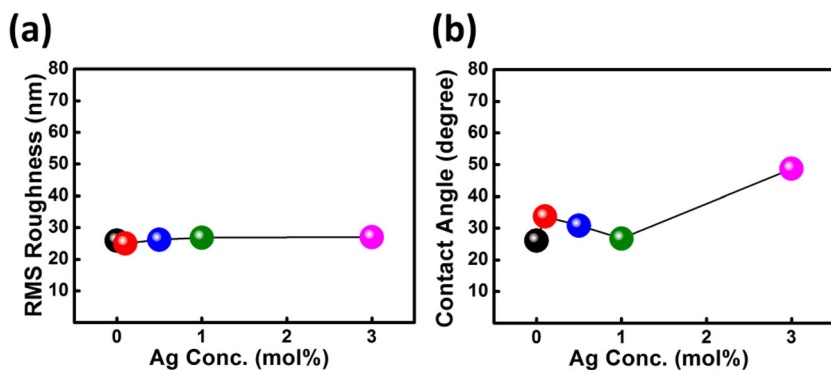


Figure 3. a) The RMS roughness distribution and b) the contact angle of the various Ag-TiO₂ layers.

We also measure the vertical conductivities of the various hole blocking layers to investigate the correlation between Ag dopant and electron transport behavior. The current density-electric field (*J-E*) curves are shown in **Figure 4**. According to the Poole-Frenkel model, the *J-E* curve is fitted by Equation (2).

$$J = \sigma_0 E \exp(\beta \sqrt{E}) \quad (2)$$

$$E = \frac{V}{L} \quad (3)$$

$$V = V_{\text{applied}} - J \cdot A \cdot r_{\text{series}} \quad (4)$$

where σ_0 and β represent the fitting parameters, σ_0 is the zero-field vertical conductivity and β is the Poole-Frenkel parameter. Electric field (*E*) is calculated by Equation (3), where *L* is the Ag-TiO₂ thickness. The voltage was through the FTO/Ag-TiO₂/Au electrode at both of the true calculation, and the voltage (*V*) is

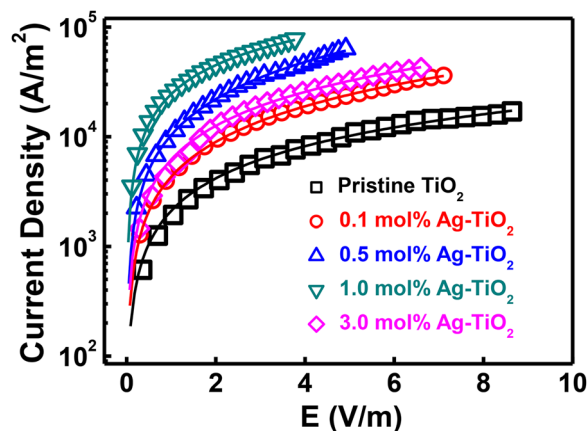


Figure 4. The various Ag-TiO₂ hole blocking layers in the *J-E* curves.

calculated by Equation (4). The r_{series} is 2 Ω for all samples and *A* is the active area of 0.04 cm². The conductivities of various Ag-TiO₂ hole blocking layers are summarized in **Table 1**. The conductivity substantially increases to 29.95 mS m⁻¹ when Ag doping level reaches 1.0 mol%. The increased conductivity for Ag-TiO₂ layer with optimal dopant level can improve the short-circuit current density (*J_{sc}*) and PCE.

Next, the photoinduced charge carrier dynamics is studied systematically using time-resolved photoluminescence (TRPL) technique. We measure the static photoluminescence (PL) and transient PL decay of the specimens with the structure of

Table 1. The conductivity of various TiO₂-based hole blocking layers.

Hole blocking layer	Conductivity [mS m ⁻¹]
Pristine TiO ₂	2.16
0.1 mol% Ag-TiO ₂	3.92
0.5 mol% Ag-TiO ₂	8.93
1.0 mol% Ag-TiO ₂	29.95
3.0 mol% Ag-TiO ₂	5.98

CH₃NH₃PbI_{3-x}Cl_x/Ag-TiO₂/FTO glass. While increasing Ag doping levels from 0.0 to 3.0 mol%, the PL quenching increases as shown in Figure 5a. This is due to the excited electron being transferred from CH₃NH₃PbI_{3-x}Cl_x to Ag-TiO₂. We also measure the transient PL decay behavior of each hole blocking layers. The results are adopted to investigate the charge transfer and separation behavior. The transient PL decay is fitted according to the exponential decay kinetics function:

$$F(t) = A_1 \exp\left(-\frac{t}{\tau_1}\right) + A_2 \exp\left(-\frac{t}{\tau_2}\right) \quad (5)$$

where: A₁ and A₂ represent time independent coefficient of amplitude fraction. τ₁ is fast decay time and τ₂ is slow decay time. Using the following equation to calculate the average PL lifetime (τ_{avg}):

$$\tau_{\text{avg}} = \frac{\sum_i A_i \tau_i}{\sum_i A_i} \quad (6)$$

The transient PL decay plots of CH₃NH₃PbI_{3-x}Cl_x/Ag-TiO₂ depicts the charge transport efficiency could be affected by Ag dopant. We summarize the measured values of τ₁, τ₂, and τ_{avg} for CH₃NH₃PbI_{3-x}Cl_x/Ag-TiO₂ in Table 2. The 3.0 mol% Ag-TiO₂ presents the shortest PL average lifetime of 16.3 ns (Figure 5b). The result shows that increasing Ag doping level could reduce the recombination. Although the Ag-TiO₂ with high dopant level exhibits high PL quenching, it lowers the PL lifetime. However, for the sample with dopant level higher than 3.0 mol%, the electrons may be caught by silver ions. This inability to transport electrons to FTO glass could affect the efficiency.

In our study, various Ag-TiO₂ layers act as the hole blocking layers in perovskite-structured solar cells. Figure 6a shows the architecture of our perovskite-structured solar cell which is composed of glass/FTO/Ag-TiO₂/CH₃NH₃PbI_{3-x}Cl_x/Spiro-OMeTAD/Ag. Figure 6b and Table 3 show the current density-voltage (J-V) curves and photovoltaic characteristics of PSCs with the various Ag-TiO₂ hole blocking layers, respectively. For the device with 1.0 mol% Ag-TiO₂ hole blocking layer, the J_{sc} is increased from 19.4 to 21.0 mA cm⁻², and the corresponding external quantum efficiency (EQE) spectra are shown in Figure 6c. The integrated EQE area of the device with 1.0 mol% Ag-TiO₂ hole blocking layer is measured from 300 to 800 nm. The absorption spectra of perovskite active layers coated on pristine TiO₂ and 1.0 mol% Ag-TiO₂ are shown in Figure S4, Supporting Information. It confirms that the absorption spectra of perovskite-structured active layer exhibit similar absorption range with EQE spectra. The open-circuit voltage (V_{oc}) increases from 0.93 to 0.97 V with increasing the dopant level to 1.0 mol% (Figure 6d). While Ag doping level is higher than 1.0 mol%, J_{sc} and V_{oc} are significantly decreased due to the lower conductivity (Figure 4) and carrier transport (Figure 5b) of Ag-TiO₂ hole blocking layer and perovskite layer. In addition, FF and PCE are improved when Ag doping level achieves 1.0 mol% (Figure 6f,g). After doping Ag with the dopant level up to 1.0 mol%, the PCE is

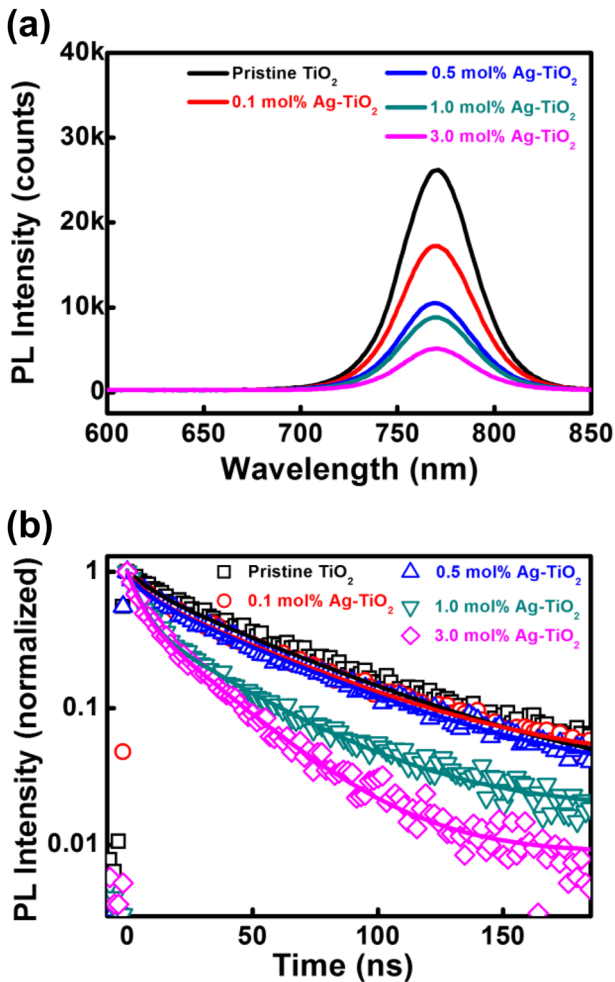


Figure 5. a) PL spectra and b) transient PL decay plots for various CH₃NH₃PbI_{3-x}Cl_x/Ag-TiO₂ measured at room temperature.

Table 2. Summary of the τ₁, τ₂, and τ_{avg} for various CH₃NH₃PbI_{3-x}Cl_x/Ag-TiO₂.

Hole blocking layer	A ₁ [%]	τ ₁ [ns]	A ₂ [%]	τ ₂ [ns]	τ _{avg} [ns]
Pristine TiO ₂	0.24	9.5	0.76	54.6	40.6
0.1 mol% Ag-TiO ₂	0.26	7.6	0.67	51.4	37.0
0.5 mol% Ag-TiO ₂	0.23	7.9	0.67	51.2	37.2
1.0 mol% Ag-TiO ₂	0.41	5.6	0.60	37.9	18.9
3.0 mol% Ag-TiO ₂	0.49	4.8	0.51	27.5	16.3

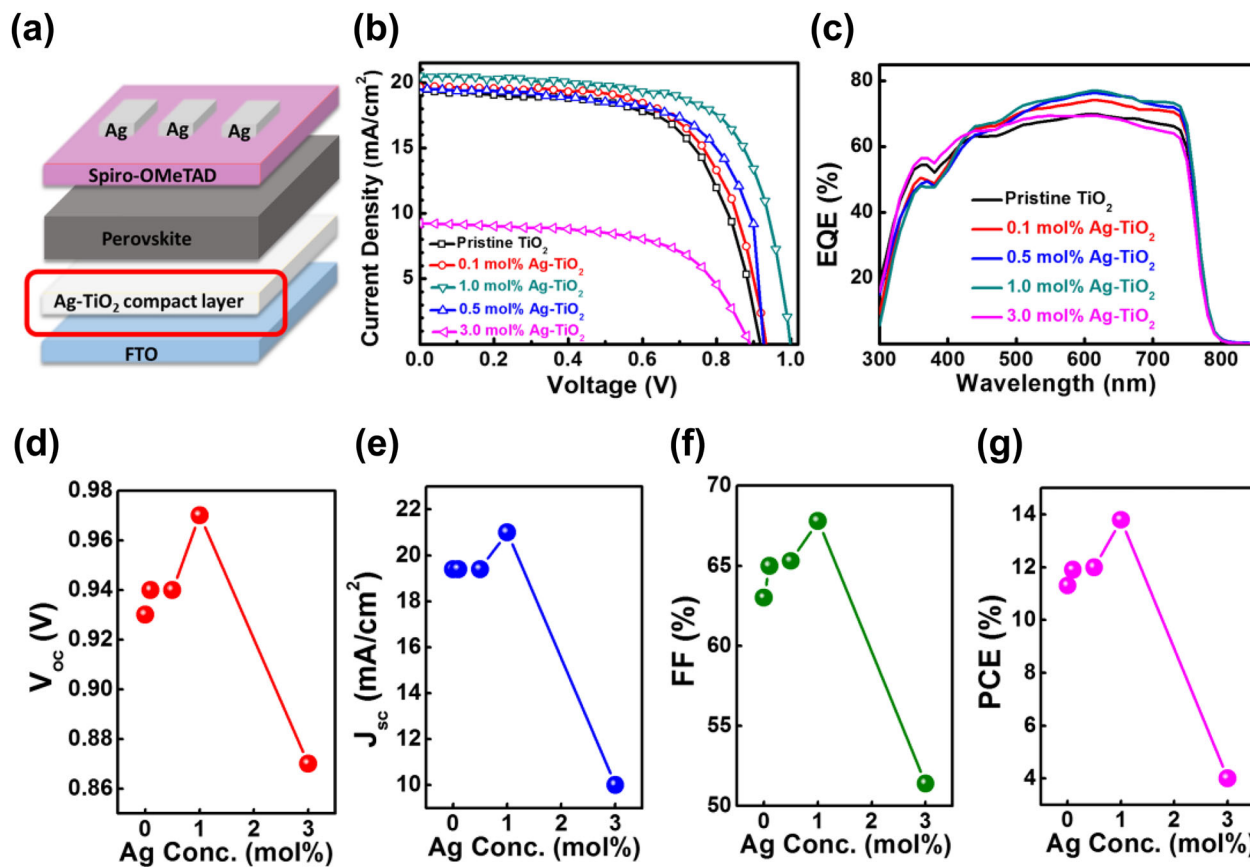


Figure 6. a) The device structure, b) J - V curves and c) the EQE curves of PSCs fabricated with different TiO_2 -based hole blocking layers, and the correlation between Ag doping levels and photovoltaic characteristics, including d) V_{oc} , e) J_{sc} , f) FF, and g) PCE.

enhanced from 11.3 to 13.8%. Therefore, the photovoltaic performance is highly connected to the charge separation and efficiency of charge transport.

The chemical compositions of 1.0 mol% Ag- TiO_2 layer is analyzed by field-emission scanning electron microscopy with energy dispersive spectroscopy (FE-SEM/EDS). To obtain high-quality signals of chemical compositions, we prepare a 1.0 mol% Ag- TiO_2 thick layer by a spin-coating method. From FE-SEM images, 1.0 mol% Ag- TiO_2 thick layer (thickness ≈ 700 nm) displays many significant fissures compared with 1.0 mol% Ag- TiO_2 thin film (thickness ≈ 90 nm). The chemical composition of 1.0 mol% Ag- TiO_2 are further measured by FE-SEM/EDS as shown in Figure S5, Supporting Information.

Table 3. The photovoltaic characteristics of PSCs fabricated with the different TiO_2 -based hole blocking layers.

Hole blocking layer	V_{oc} [V]	J_{sc} [mA cm^{-2}]	FF [%]	PCE [%]
Pristine TiO_2	0.93 ± 0.03	19.4 ± 0.2	62.7 ± 1.8	11.3 ± 0.3
0.1 mol% Ag- TiO_2	0.94 ± 0.01	19.4 ± 0.2	64.9 ± 1.3	11.9 ± 0.4
0.5 mol% Ag- TiO_2	0.94 ± 0.02	19.4 ± 0.4	65.3 ± 1.7	12.0 ± 0.3
1.0 mol% Ag- TiO_2	0.97 ± 0.04	21.0 ± 0.6	67.8 ± 3.3	13.8 ± 0.7
3.0 mol% Ag- TiO_2	0.87 ± 0.02	10.0 ± 4.3	51.4 ± 17.5	4.0 ± 1.0

Table S1, Supporting Information records the ratios of Ag/Ag+Ti at different positions of 1.0 mol% Ag- TiO_2 thick layer, and it indicates that Ag distributes uniformly in TiO_2 . In addition, the chemical composition of Ag- TiO_2 thin layer is further investigated by X-ray photoelectron spectra (XPS). For pristine TiO_2 and various Ag- TiO_2 , the electron-binding energy of Ti 2p, O 1s, C 1s, and Ag 3d shows no significant shift (Figure S6a-d, Supporting Information). The atomic ratios of Ag/Ag+Ti for various Ag- TiO_2 layers are shown in Table S2, Supporting Information. The XPS analysis indicates that the atomic ratios of Ag/Ag+Ti are close to theoretical values for various Ag- TiO_2 .

We use the photo-assisted Kelvin probe force microscopy (KPFM) to monitor the surface potentials of pristine TiO_2 and 1.0 mol% Ag- TiO_2 layers, and the measurement is performed in the dark and under illumination as shown in Figure 7. We measured the topography (Figure 7a,b) and surface potential (Figure 7e,f) of the perovskite-structured active layer coated on two kinds of TiO_2 -based layer. The cross-section of topography for both samples are shown in Figure 7c,d, and their roughness is similar. The contact potential difference (CPD) is measured by conductive tips under ambient condition, in the dark and under illumination, respectively. The perovskite-structured active layer absorbs light. Then, the excitons are generated and immediately divided into electrons and holes. The electrons were injected into

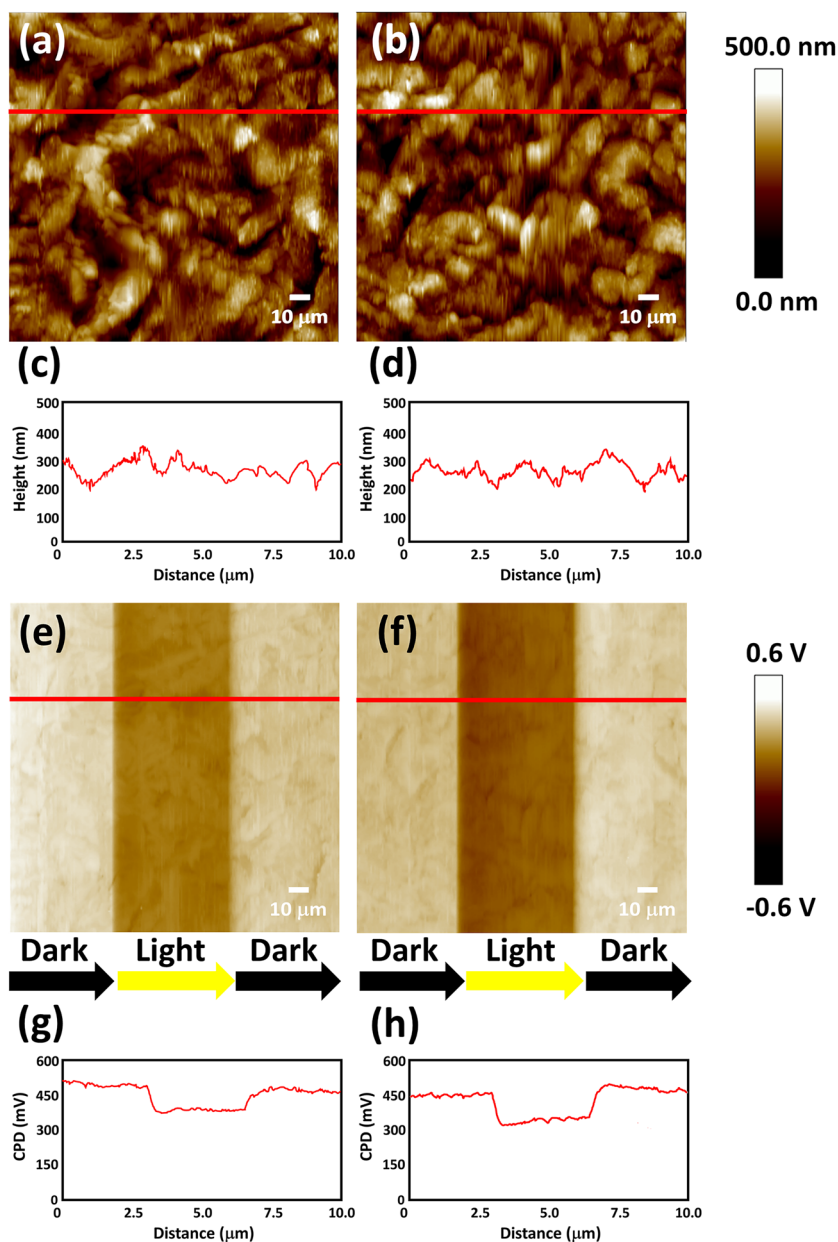


Figure 7. a,b) The surface images and c,d) the cross-section images measured by AFM. e,f) The surface potential mapping and g,h) the cross-section images measured by KPFM for pristine TiO₂ (a,c,e,g) and 1.0 mol% Ag-TiO₂ (b,d,f,h).

the TiO₂ layer and changed the work function. The CPD is calculated by:

$$V_{CPD} = \frac{SP_{tip} - SP_{sample}}{-e} \quad (7)$$

where: SP_{tip} and SP_{sample} are surface potentials of tip and sample, and e is electric charge. Under illumination, the change of CPD (284.42 mV) for 1.0 mol% Ag-TiO₂ is higher than that of pristine TiO₂ (214.84 mV), shown in Figure 7g and h. The perovskite-structured film with 1.0 mol% Ag-TiO₂ layer exhibited large surface potential under illumination. These

results indicate that the Ag dopant can increase the charge transport effect, which can be advantageous due to the improved photovoltaic performance.

The light intensity-dependent $J-V$ characteristic is used to observe the charge recombination behavior of 1.0 mol% Ag-TiO₂ hole blocking layer. The light-intensity dependent J_{SC} and V_{OC} characteristics is fitted linear as shown in Figure 8a,b. For the V_{OC} dependence on light intensity, the fitted slopes of pristine TiO₂ and 1.0 mol% Ag-TiO₂ hole blocking layers are $2.30 \frac{k_B T}{q}$ and $1.89 \frac{k_B T}{q}$, respectively. Where: k_B is the Boltzmann constant, T is the absolute temperature and q is the elementary charge. When the slope value is more than or equal to 2, the trap-assisted recombination tend to domain in PSCs. Hence, the slope of $1.89 \frac{k_B T}{q}$ for 1.0 mol% Ag-TiO₂ hole blocking layer indicates that it could hinder the trap-assisted recombination.

For hysteresis measurement, the $J-V$ curves and photovoltaic performance of the champion device with pristine TiO₂ and 1.0 mol% Ag-TiO₂ hole blocking layer are shown in Figure 9a,b and Table 4, with scan direction in reverse scan and forward scan. The hysteresis index (HI) is defined by the Equation (8).^[38]

$$HI = \frac{J_{RS}(0.8V_{oc}) - J_{FS}(0.8V_{oc})}{J_{RS}(0.8V_{oc})} \quad (8)$$

The PCE of PSC based on the pristine TiO₂ hole blocking layer on the forward scan is 7.5%, lower than that of 11.6% on the reverse scan. The PCE of PSC based on 1.0 mol% Ag-TiO₂ hole blocking layer on the forward scan is 10.3%, and is 14.1% on the reverse scan. Thus, doping optimal silver concentration into TiO₂ (≈ 1.0 mol%) can decrease the HI index from 0.92 to 0.52, and it also can enhance the PCE on both the reverse scan and the forward scan. The hysteresis phenomenon could be due to the carrier flux unbalance in planar n-i-p PSCs.^[37,39–40] Doping optimal silver concentration into TiO₂ could promote the electron transporting rate, thus achieving the electrons and holes flux balance.

Furthermore, we conduct the stability test of PSCs based on pristine TiO₂ and 1.0 mol% Ag-TiO₂ as shown in Figure 10. The PSCs with 1.0 mol% Ag-TiO₂ were stored in glovebox system with nitrogen atmosphere humidity less than 0.1 ppm and oxygen less than 0.1 ppm. After 720 h, the PSCs with 1.0 mol% Ag-TiO₂ hole blocking layers maintain the initial PCE about 83.0%. We suggest that the degradation of PSCs is due to the perovskite active layer which is extremely sensitive to moisture.^[41] The other reason could be due to the leakage of additive in the spiro-OMeTAD which leads to the progressive decrease of the conductivity. The additive in the spiro-OMeTAD has been

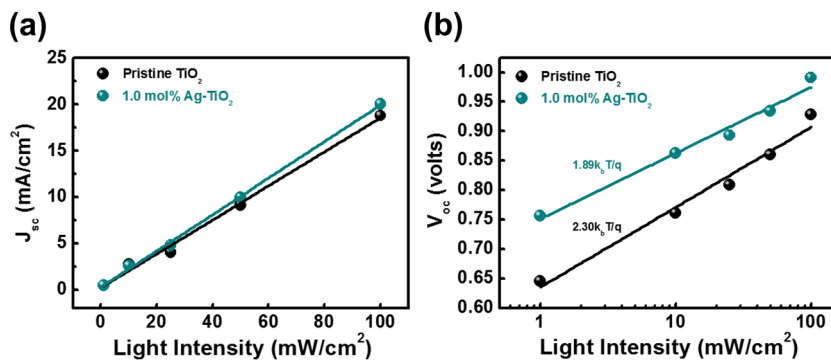


Figure 8. The different light intensity for a) J_{sc} and b) V_{oc} of perovskite-structured solar cell with pristine TiO₂ and 1.0 mol% Ag-TiO₂ hole blocking layer.

identified as one of the primary sources of instability in the solar cell.^[42] Our device with high stability could be attributed to the effective charge separation efficiency facilitated by Ag-TiO₂ hole blocking layer. Therefore, the improved photovoltaic performance contributes to the increased stability of perovskite-structured solar cells.

As we mentioned in previous results, the optimal energy band alignment between active layer and hole blocking layer is important for PSCs. In order to check the position of the valence band (VB) and conduction band (CB) in pristine TiO₂ and 1.0 mol% Ag-TiO₂ hole blocking layer, we use the ultraviolet photoelectron spectroscopy (UPS) to investigate (Figure S7, Supporting Information). The energy level diagram (Figure S7a, Supporting Information) is calculated by the UPS analysis and UV-Vis analysis. The work function (WF) of pristine TiO₂ layer and 1.0 mol% Ag-TiO₂ layer are obtained by subtracting the cut-off binding energy with the photon energy (21.22 eV) and the values are 5.33 eV and 5.41 eV, respectively (Figure S7b,c, Supporting Information). The Fermi levels (E_f) of pristine TiO₂ layer and 1.0 mol% Ag-TiO₂ layer are 1.46 eV and 1.24 eV, respectively (Figure S7d,e, Supporting Information). Hence, the calculated VB of pristine TiO₂ layer and 1.0 mol% Ag-TiO₂ layer are -6.79 eV and -6.65 eV, respectively. The CB of pristine TiO₂ layer and 1.0 mol% Ag-TiO₂ layer are -3.03 eV and -2.91 eV, respectively. The calculated results indicate that Ag-TiO₂ could result in the upwards shift of VB and CB, therefore, it could

effectively enhance the band structure of TiO₂ and further facilitate the charge carrier behavior.

3. Conclusion

We successfully fabricated various Ag-TiO₂ as the hole blocking layer for the high-performance PSCs. The bandgap of Ag-TiO₂ decreases as dopant levels increase. The average V_{oc} increases from 0.93 to 0.97 V and the average J_{sc} increases from 19.4 to 21.0 mA cm⁻², when Ag doping level reaches 1.0 mol%. The increased V_{oc} and J_{sc} are due to the optimal band alignment, which could increase the electron injection. In addition, the

optimal Ag doping level, at ≈ 1.0 mol%, for PSCs could reduce the hysteresis behavior, with HI decreasing from 0.92 to 0.52. This silver doping can also enhance the PCE, and its PCE of the champion device with 1.0 mol% Ag-TiO₂ hole blocking layer reaches as high as 14.1%.

4. Experimental Section

Preparation of Ag-TiO₂ Precursor Solution: For the titanium precursor solution, titanium tetraisopropoxide (Ti(OCH(CH₃)₂)₄, TTIP, >97%, Sigma-Aldrich) was added to ethanol. In another beaker, 2.0 M HNO₃ solution was added to ethanol, and then mixed with Ti precursor solution. Silver nitrate (AgNO₃) was dissolved in ethanol as Ag precursor solution until it was completely dissolved. Then, the Ag precursor solution with different stoichiometric ratios was mixed with titanium precursor solution. As such, the Ag-TiO₂ precursor solution was finished preparing.

Preparation of CH₃NH₃PbI_{3-x}Cl_x Perovskite Precursor Solution: The methylammonium iodide (CH₃NH₃I) was synthesized according to our previous study.^[43] Then, the MAI must be dried at 50 °C in a vacuum oven for 24 h. The CH₃NH₃PbI_{3-x}Cl_x perovskite precursor solution was prepared by mixing MAI and lead chloride (PbCl₂, 99.999%, Sigma-Aldrich) with the stoichiometric ratio at 0.9 M in 1.0 mL dimethylformamide (HCON(CH₃)₂, DMF, anhydrous, 99.8%, ACROS).

Fabrication of Perovskite-Structured Solar Cells: The Ag-TiO₂ precursor solution was deposited on the FTO glass (7Ω, FrontMaterials Co. Ltd.) by spin coating and calcined at 550 °C to form the Ag-TiO₂ hole blocking layer. The CH₃NH₃PbI_{3-x}Cl_x solution was spin-coated on Ag-TiO₂ hole blocking layer, then spiro-OMeTAD solution was spin-coated over CH₃NH₃PbI_{3-x}Cl_x layer.^[44] Finally, 100 nm thickness silver electrode was thermally evaporated on top of the device through a shadow mask with 0.09 cm² active area. The PCE of various types of PSCs were evaluated statistically by averaging 18 separated photovoltaic devices.

Characterization: The crystal structure of various Ag-TiO₂ hole blocking layers were measured by the x-ray diffractometer (XRD, Bruker, D2 phaser with Xflash 430, Germany). The UV-Vis absorption of various Ag-TiO₂ hole blocking layers were measured by UV-Vis spectrometer (V-730, Jasco). The surface microstructure of various Ag-TiO₂ hole blocking layers were observed by SEM (SNE-4500M, SEC). The surface microstructure images and atomic ratio of pristine TiO₂ and 1.0 mol% Ag-TiO₂ layer were measured by FE-SEM (SU8010, Hitachi) equipped with EDS (XFlash Detector 5030, Bruker AXS). AFM

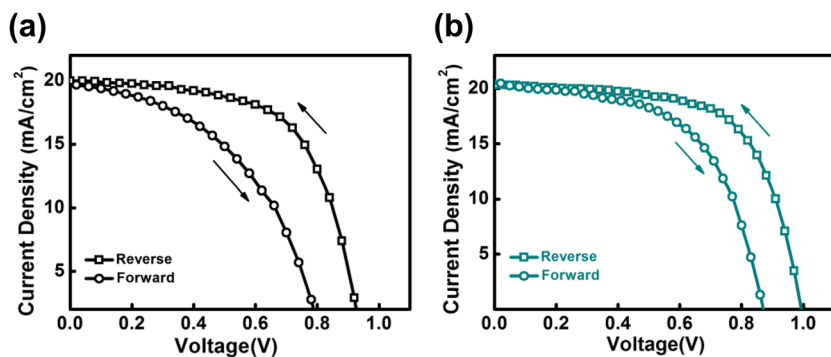


Figure 9. J - V curves of the PSCs based on the different hole blocking layers, a) pristine TiO₂ and b) 1.0 mol% Ag-TiO₂, on the reverse scan and the forward scan.

Table 4. The photovoltaic performance of PSCs base on the different hole blocking layers on the reverse scan and the forward scan.

Hole blocking layer	Scan direction	V_{oc} [V]	J_{sc} [mA cm^{-2}]	FF [%]	PCE [%]	HI
Pristine TiO_2	Reverse	0.94	19.9	62.4	11.7	1.08
	Forward	0.80	19.7	46.8	7.5	
1.0 mol% Ag- TiO_2	Reverse	1.00	20.5	68.7	14.1	0.52
	Forward	0.90	20.5	55.5	10.3	

measured the topographic images and roughness analysis of $\text{CH}_3\text{NH}_3\text{PbI}_{3-x}\text{Cl}_x$ films coated on the various Ag- TiO_2 hole blocking layers. The contact angles of various Ag- TiO_2 hole blocking layers were measured using water droplets measurement by contact angle goniometer (1005B, Sindatek Instruments Co. Ltd.). The photoluminescence (PL) measurements of $\text{CH}_3\text{NH}_3\text{PbI}_{3-x}\text{Cl}_x$ film coated with various Ag- TiO_2 hole blocking layers were taken under 440 nm continuous wave diode laser (DongWoo Optron Co. Ltd.). The TRPL spectra of the perovskite-structured film coated with various Ag- TiO_2 hole blocking layers were observed using time-correlated single photon counting (TCSPC) using 440 nm pulse laser (WELLS-001 FX, DongWoo Optron Co. Ltd.). The J - V curves of various PSCs with different TiO_2 -based hole blocking layers were recorded by the computer-controlled digital source meter (Keithley 2410, Keithley, OH, USA) under 1.0 sun illumination (100 mW cm^{-2} , AM 1.5G). The solar-simulated AM 1.5 sunlight was generated using irradiation (Newport-69920, 100 mW cm^{-2}) calibrated with a silicon reference cell (Oriel P/N 91150V, VLSI standards) with KG-5 visible color filter. The characteristics of EQE spectra for PSCs with the different TiO_2 -based hole blocking layers were analyzed (EQE-R-3011, Enli Technology Co. Ltd.). The chemical composition of various Ag- TiO_2 layer were obtained by X-ray photoelectron spectrometer (K-Alpha X-ray photoelectron spectrometer, Thermo Fisher Scientific). For KPFM measurement, the CPD of perovskite-structured film coated with the various Ag- TiO_2 were analyzed by a KPFM measurement system (Digital Instruments Dimension, 3100). For hysteresis measurement, the applied bias was swept from +1.2 V to -0.1 V on the reverse scan and from +0.1 V to -1.2 V on the forward scan. The measured delta V and delay time for the reverse and the forward scan are -0.04 V, 0.04 V and 10 s, respectively. The energy levels of pristine TiO_2 layer and 1.0 mol% Ag- TiO_2 layer were measured by ultraviolet photoelectron spectroscopy (PHI 5000 VersaProbe, ULVAC-PHI) using an ultraviolet light source of He I emission (21.2 eV, B50 W) and take-off angle of 90° .

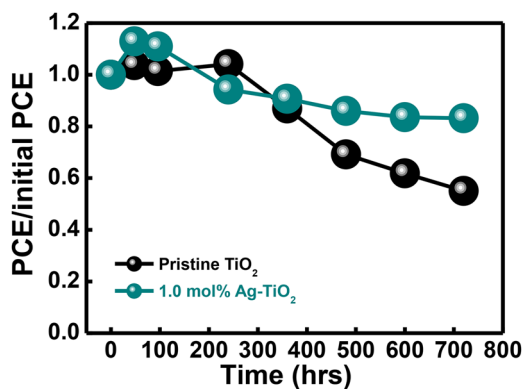


Figure 10. The stability of the PSCs based on pristine TiO_2 and 1 mol% Ag- TiO_2 hole blocking layers up to 720 h.

Supporting Information

Supporting Information is available from the Wiley Online Library or from the author.

Acknowledgments

The authors appreciate Dr. Ming-Tao Lee group (BL-13A1) at NSRRC for Synchrotron X-ray analysis and Prof. Jing-Jong Shyue at Academia Sinica for UPS analysis. The authors would like to thank the financial support of Chang Gung Memorial Hospital, Linkou (BMRPC74) and Ministry of Science and Technology, Taiwan (Grant No. 106-2221-E-182-057-MY3, 106-2632-E-182-001, and 106-2119-M-002-030).

Conflict of Interest

The authors declare no conflict of interest.

Keywords

Ag doping, hole blocking layer, Kelvin probe force microscopy, perovskite solar cells, TiO_2

Received: March 9, 2018

Revised: May 3, 2018

Published online:

- [1] A. Kojima, K. Teshima, Y. Shirai, T. Miyasaka, *J. Am. Chem. Soc.* **2009**, *131*, 6050.
- [2] http://www.nrel.gov/ncpv/images/efficiency_chart.jpg.
- [3] W. S. Yang, B. W. Park, E. H. Jung, N. J. Jeon, Y. C. Kim, D. U. Lee, S. S. Shin, J. Seo, E. K. Kim, J. H. Noh, S. I. Seok, *Science* **2017**, *356*, 1376.
- [4] Y. Kato, L. K. Ono, M. V. Lee, S. Wang, S. R. Raga, Y. Qi, *Adv. Mater. Interfaces* **2015**, *2*, 1500195.
- [5] J. K. Kim, S. U. Chai, Y. Cho, L. Cai, S. J. Kim, S. Park, J. H. Park, X. Zheng, *Small* **2017**, *13*, 1702260.
- [6] N. J. Jeon, J. H. Noh, W. S. Yang, Y. C. Kim, S. Ryu, J. Seo, S. I. Seok, *Nature* **2015**, *517*, 476.
- [7] N. J. Jeon, J. H. Noh, Y. C. Kim, W. S. Yang, S. Ryu, S. I. Seok, *Nature Materials* **2014**, *13*, 897.
- [8] Y. Cheng, X. Xu, Y. Xie, H. W. Li, J. Qing, C. Ma, C. S. Lee, F. So, S. W. Tsang, *Solar RRL* **2017**, *1*, 1700097.
- [9] X. Xu, C. Ma, Y. Cheng, Y. M. Xie, X. Yi, B. Gautam, S. Chen, H. W. Li, C. S. Lee, F. So, S. W. Tsang, *J. Power Sources* **2017**, *360*, 157.
- [10] D. W. Liu, I. C. Cheng, J. Z. Chen, H. W. Chen, K. C. Ho, C. C. Chiang, *J. Opt. Soc. Am.* **2012**, *20*, A168.
- [11] J. van de Lagemaat, N. G. Park, A. J. Frank, *J. Phys. Chem. B* **2000**, *104*.

- [12] H. Yu, S. Zhang, H. Zhao, G. Will, P. Liu, *Electrochim. Acta* **2009**, *54*, 1319.
- [13] T. Zhu, S. P. Gao, *J. Phys. Chem. C* **2014**, *118*, 11385.
- [14] Z. Liu, Q. Chen, Z. Hong, H. Zhou, X. Xu, N. De Marco, P. Sun, Z. Zhao, Y. B. Cheng, Y. Yang, *ACS Appl. Mater. Interfaces* **2016**, *8*, 11076.
- [15] K. Zhang, J. H. Park, *J. Phys. Chem. Lett.* **2017**, *8*, 199.
- [16] G. S. Han, Y. H. Song, Y. U. Jin, J. W. Lee, N. G. Park, B. K. Kang, J. K. Lee, I. S. Cho, D. H. Yoon, H. S. Jung, *ACS Appl. Mater. Interfaces* **2015**, *42*, 23521.
- [17] B. Liu, H. M. Chen, C. Liu, S. C. Andrews, C. Hahn, P. Yang, *J. Am. Chem. Soc.* **2013**, *135*, 9995.
- [18] L. T. Tseng, X. Luo, N. Bao, J. Ding, S. Li, J. Yi, *Mater. Lett.* **2016**, *170*, 142.
- [19] X. Liu, K. W. Tsai, Z. Zhu, Y. Sun, C. C. Chueh, A. Jen, *Adv. Mater. Interfaces* **2016**, *3*, 1600122.
- [20] Y. Shi, Y. Xing, Y. Li, Q. Dong, K. Wang, Y. Du, X. Bai, S. Wang, Z. Chen, T. Ma, *J. Phys. Chem. C* **2015**, *119*, 15868.
- [21] Y. Li, W. Sun, W. Yan, S. Ye, H. Peng, Z. Liu, Z. Bian, C. Huang, *Adv. Funct. Mater.* **2015**, *25*, 4867.
- [22] M. Lyu, J. H. Yun, R. Ahmed, D. Elkington, Q. Wang, M. Zhang, H. Wang, P. Dastoor, L. Wang, *J. Colloid Interface Sci.* **2015**, *453*, 9.
- [23] M. Che, Y. Fang, J. Yuan, Y. Zhu, Q. Liu, J. Song, *Int. J. Electrochem. Sci.* **2017**, *12*, 1064.
- [24] Z. L. Zhang, J. F. Li, X. L. Wang, J. Q. Qin, W. J. Shi, Y. F. Liu, H. P. Gao, Y. L. Mao, *Nanoscale Res. Lett.* **2017**, *12*, 43.
- [25] X. Zhang, Z. Bao, X. Tao, H. Sun, W. Chen, X. Zhou, *RSC Adv.* **2014**, *4*, 64001.
- [26] M. C. Wu, S. H. Chan, M. H. Jao, W. F. Su, *Sol. Energy Mater. Sol. Cells* **2016**, *157*, 447.
- [27] W. Wang, H. Zheng, Y. Liu, J. Sun, L. Gao, *J. Nanosci. Nanotechnol.* **2016**, *16*, 12768.
- [28] M. M. A. Latif, J. Xu, J. Yao, S. Dai, *Mater. Sci. Forum* **2017**, *896*, 18.
- [29] J. Liu, J. Zhang, Y. X. Lu, Z. Hu, Y. Zhu, *Electrochim. Acta* **2016**, *195*, 143.
- [30] Y. Li, Y. Guo, Y. Li, X. Zhou, *Electrochim. Acta* **2016**, *200*, 29.
- [31] H. Kim, G. S. Han, W. M. Seong, J. W. Lee, B. J. Kim, N. G. Park, K. S. Hong, S. Lee, H. S. Jung, *ChemSusChem* **2015**, *8*, 2392.
- [32] A. K. Gupta, P. Srivastava, L. Bahadur, *Appl. Phys. A* **2016**, *122*, 724.
- [33] K. Usha, P. Kumbhakar, B. Mondal, *Mater. Sci. Semicond. Process.* **2016**, *43*, 17.
- [34] C. H. Wu, K. S. Lin, C. H. Yang, *ECS Meeting Abstracts* **2014**, MA2014-02, 1946.
- [35] S. I. Mogal, V. G. Gandhi, M. Mishra, S. Tripathi, T. Shripathi, P. A. Joshi, D. O. Shah, *Ind. Eng. Chem. Res.* **2014**, *53*, 5749.
- [36] Z. Sarteep, A. E. Pirbazari, M. A. Aroon, *J. Water Environ. Nanotechnol.* **2016**, *1*, 135.
- [37] J. H. Heo, M. S. You, M. H. Chang, W. Yin, T. K. Ahn, S. J. Lee, S. J. Sung, D. H. Kim, S. H. Im, *Nano Energy* **2015**, *15*, 530.
- [38] H. S. Kim, N. G. Park, *J. Phys. Chem. Lett.* **2014**, *5*, 2927.
- [39] H. J. Snaith, A. Abate, J. M. Ball, G. E. Eperon, T. Leijtens, N. K. Noel, S. D. Stranks, J. T. W. Wang, K. Wojciechowski, W. Zhang, *J. Phys. Chem. Lett.* **2014**, *5*, 1511.
- [40] V. Trifiletti, N. Manfredi, A. Listorti, D. Altamura, C. Giannini, S. Colella, G. Gigli, A. Rizzo, *Adv. Mater. Interfaces* **2016**, *3*, 1600493.
- [41] B. Suarez, V. G. Pedro, T. S. Ripolles, R. S. Sanchez, L. Otero, I. Mora-Sero, *J. Phys. Chem. Lett.* **2014**, *5*, 1628.
- [42] J. A. Christians, P. A. M. Herrera, P. K. Kamat, *J. Am. Chem. Soc.* **2015**, *137*, 1530.
- [43] C. Y. Chang, C. Y. Chu, Y. C. Huang, C. W. Chang, S. Y. Chen, C. A. Chao, C. Y. Chao, W. F. Su, *ACS Appl. Mater. Interfaces* **2015**, *7*, 4955.
- [44] D. Liu, T. L. Kelly, *Nat. Photonics* **2014**, *8*, 133.